Communication

Local Electrical Response in Alkaline-Doped Electrodeposited CuInSe2/Cu Films

Javier A. Barón-Miranda [1], Octavio Calzadilla [2], Liliana E. Arvizu-Rodríguez [3], Jose L. Fernández-Muñoz [4], Cesia Guarneros-Aguilar [5], Fabio Chale-Lara [1], Ulises Páramo-García [3] and Felipe Caballero-Briones [1,*]

[1] Instituto Politécnico Nacional, Materiales y Tecnologías para Energía, Salud y Medioambiente (GESMAT), CICATA Altamira. Km.14.5 Carretera Tampico-Puerto Industrial, 89600 Altamira, Mexico; armandobaron1150@gmail.com (J.A.B.-M.); fchale@ipn.mx (F.C.L.)

[2] Facultad de Física, Universidad de La Habana, San Lázaro y L, Vedado, 10400 La Habana, Cuba; calza@fisica.uh.cu

[3] División de Estudios de Posgrado e Investigación, Instituto Tecnológico de Cd. Madero, Tamaulipas, Mexico; liliarvizurdz@gmail.com (L.E.A.R.); uparamo@itcm.edu.mx (U.P.-G.)

[4] Instituto Politécnico Nacional, CICATA Legaria. Calzada Legaria 396 Col. Irrigación, 11500, CdMx, Mexico; jlfernandez@ipn.mx   Country should be written in English, please revise

[5] CONACYT-Instituto Politécnico Nacional, GESMAT-CICATA Altamira 89600, Mexico; cguarnerosag@conacyt.mx

* Correspondence: fcaballero@ipn.mx; Tel.: +52-55-57-296300 ext 87508

Abstract: The local electrical response in alkaline-doped CuInSe2 films prepared by single-step electrodeposition onto Cu substrates was studied by current-sensing atomic force microscopy. The CuInSe2 (CIS) films were prepared from single baths containing the dopant ions (Li, Na, K or Cs) and were studied by X-ray diffraction, scanning electron microscopy, energy dispersive X-ray spectroscopy and photocurrent response. Increased crystallinity and surface texturing as the ion size increased were observed, as well as an enhanced photocurrent response in Cs-doped CIS. Li- and Na-doped films had larger conductivity than the undoped film while the K- and Cs-doped samples displayed shorter currents and the current images indicated strong charge accumulation in the K- and Cs-doped films, forming surface capacitors. Corrected current-sensing AFM IV curves were adjusted with the Shockley equation.

Keywords: CuInSe2 electrodeposition; alkaline doping; current sensing atomic force microscopy

1. Introduction

CuInSe2 (CIS) is a p-type semiconductor of interest for solar cells [1], photocatalysis [2] and water splitting [3]. The electrical properties of CIS depend on its defect chemistry [4]. With respect to alkaline doping, Na incorporation after deposition leads to enhanced current transport, attributed to Se vacancy passivation [5], but also to the introduction of acceptor defects, the elimination of InCu donors or the elimination of defects at grain boundaries [6]; when incorporated during growth, Na affects Cu homogeneity on a microscopic level, leading to lower charge carrier mobilities [7]. In the case of Li, a small contribution to the valence or conduction band states was found, although an increase in the band gap was attributed to effects on Se p-orbitals due to Li ionicity [8]. For K-doping in Cu(In,Ga)Se2, a reduced minority carrier lifetime, and poorer and temperature-dependent collection of photogenerated charge carriers were observed [6], although recent data contradict these observations [9,10]: K-doping in Cu(In,Ga)Se2 (CIGS) films, not yet introduced during deposition or by a postdeposition treatment, increases the cell efficiency by reducing Cu at the CIGS surface upon formation of In and Ga oxides, although detrimental effects of a proposed KInSe2 compound on the electrical properties have been mentioned in [9]. Finally, in a study of anodic p-Cu2O films doped with Li, Na, K and Cs [11], a shift of the acceptor level position together with an increase of the carrier

density and electrical conductivity and a reduction in the photocurrent response with the dopant ion size was observed. First-principles calculations indicate a net attractive interaction for Li−O bonds, a slightly repulsive interaction for Na−O, and a net repulsive interaction for K−O and Cs−O, respectively [11].

On the other hand, current-sensing atomic force microscopy is a powerful tool to observe the local electrical properties and electrically active sites at grains and grain boundaries. Its usefulness has been tested in many photovoltaic devices, for example in assessing photoactivity in $CuInSe_2/Au$ nanowire arrays [12], and in studying the current routes in polycrystalline CIS and CIGS [13]. However, the exploiting of CAFM-IV curves in CIS and doped CIS has been scarcely done. CAFM-IV curves carry additional information on the surface states and grain boundaries and physical information such as the barrier height, series resistance and ideality factor of the diode-like junction between the tip and sample which can be modeled with the appropriate model [14]. In this work, $CuInSe_2/Cu$ films were prepared by electrodeposition and Li, K, Na or Cs ions were added during the growth. The nanoelectrical and photocurrent responses were studied and interpreted in terms of the dopant effects on the crystalline and electronic structures.

2. Materials and Methods

Electrodeposition of $CuInSe_2$ films was done at pH 2 onto chemically polished, single-sided PC boards (copper laminated onto an FR4 glassfiber-resin board) using an Autolab 302 station with the Cu-cladded board as working electrode, Pt gauze as counter electrode and a Ag/AgCl (Silver/Silver Chloride) reference electrode [15]. The concentration of Cu^{2+}, Se^{2-} and In^{3+} solutions were 0.1 mM, 0.1 mM and 0.2 mM, respectively, using $CuSO_4$ (99% Sigma Aldrich, Sigma-Aldrich Química, S.L.,Toluca, Mexic), SeO_2 (98% Sigma Aldrich) and $In2(SO_4)_3$ (98% Sigma Aldrich) as precursors. Dopant solutions of 0.1 M LiOH (98% Sigma Aldrich), 0.1 M NaOH (99% Sigma Aldrich), 0.1 M KOH (90% Sigma Aldrich) and 50% CsOH solution (99% Sigma Aldrich) were added in proper volume to achieve a 1:10 dopant/Cu^{2+} ratio in the bath. The substrates were introduced into the electrolyte 2 min before applying potential to form a reddish Cu_2Se buffer layer, this layer has been found as necessary to ensure adhesion; then the potential was swept from open circuit potential (OCP) to −1500 mV at 5 mV s^{-1} and maintained during 15 min. Finally, the samples were rinsed with deionized water and dry under N_2 stream. X-ray diffractograms were acquired in a Bruker D8 Advance in the Bragg-Brentano geometry using CuKα radiation. Photocurrent response was recorded in the constant wave mode using 0.1 M $NaNO_3$ as electrolyte, sweeping the potential at a 5 mVs^{-1} rate [16]. Illumination was done using a 75 W quartz tungsten halogen lamp located 10 cm away from the sample, illuminating a 1.2 cm^2 area. Scanning electron microcopy and energy dispersive X-ray spectroscopy (EDS) were done in an EDAX/Quanta microscope operating at 20 kV. Current sensing atomic force microscopy (CAFM) was done in a Dimension (Veeco Instruments, Plainview, NY, USA) microscope using solid Pt/Ir bend wire tips (RMN 25Pt300B, Bruker, Camarillo, CA, USA). Topographic and current images were acquired at +100 and −100 mV bias and the IV curves were recorded after imaging a conductive site; the potential was applied to the sample holder while keeping tip grounded. Three points in the sample were imaged and each reported curve is the average of at least 50 measurements. A description of the curve analysis in presented in Supplementary Information.

3. Results and Discussion

3.1. Morphology, Composition and Structural Characterization

Figure 1 presents the SEM images at two different magnifications of the prepared CIS and alkaline-doped CIS films and the atomic composition at the side of the SEM images. EDS spectra were obtained at the grain surface, the grain edges and at the apparent bottom of the images to assess the growth dynamics. Cu, In, Se and O were detected in all the films and Cu in large concentration arose from the substrate.
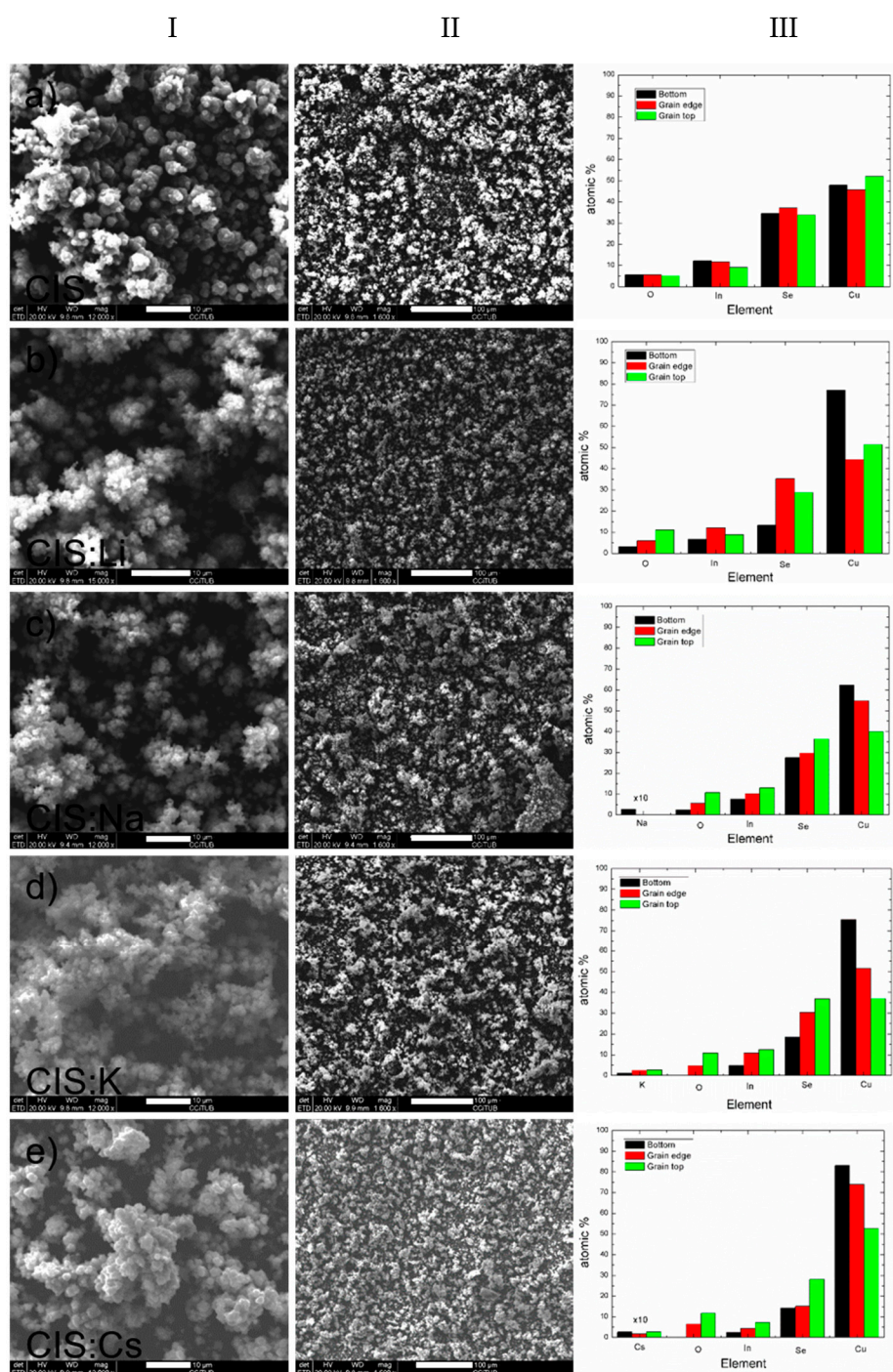
Figure 1. SEM micrographs obtained at (I) 12000× and (II) 1500×; (III) EDS data of the a) CIS, b) CIS:Li, c) CIS:Na, d) CIS:K and e) CIS:Cs films obtained at the image apparent bottom (black bar), grain edge (red bar) and grain top (green bar).

SEM images indicate an island type of growth with continuous grain formation and no coalescence. Li-, Na- and K-doped films are porous, suggesting H_2 evolution. CIS and CIS:Cs films are consist in defined grains, with a rounded (CIS) and faceted (CIS:Cs) aspect, respectively. The absence of H_2 evolution in the Cs-doped film can be explained in the light of its large electron affinity, causing catalytic water hydrolysis, with the subsequent local pH increment [17].

The composition of the undoped CIS film is almost constant through the film depth as the analysis of the composition measured at different parts of the images indicates. The selenium excess with respect to the In:Se 1:2 ratio is attributed to the Cu_2Se buffer layer. The maximum contents of

detectable alkaline ions (Na, K and Cs) were Na 0.25 at.%, K 2.80%, and Cs 0.28%, respectively. The higher amount of K is intriguing, even though K segregation to the grain boundaries has been reported; another explanation for the abnormally high K contents would be the formation of a $KInSe_2$ phase which has been suggested as responsible for the detriment in the electrical properties of K-doped $Cu(In,Ga)Se_2$ films [6,9,10]. This assumption could be related to the increment in the Se/Cu ratio in the K-doped film together with the K increase at the film top observed by EDS. In the case of Na-doped CIS, Na was only detected at the film bottom, in contrast with K and Cs which were detected in all the film. The highest concentration of Cs is at the top of the film, suggesting surface accumulation due to its large ion size [11]. The oxygen concentration increases in all the films from the bottom to the top, except for the undoped films, indicating progressive oxidation during film growth, promoted by the alkaline ions [5], and confirming Li incorporation into the film, undetectable by EDS.

Figure 2 shows the X-ray diffractograms of the deposited films, separated into A and B ranges for an easier discussion of the observed diffraction peaks.
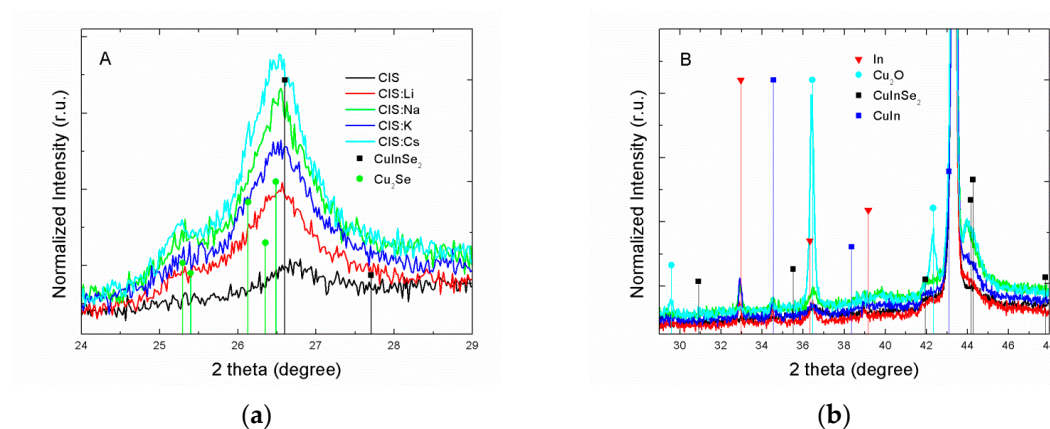

(**a**)   (**b**)

Figure 2. X-ray diffractograms of the prepared films.

Figure 2A displays the XRD in the region 2θ 24°–29°, around the main peak of tetragonal CIS. In this region, the patterns present a wide peak associated with tetragonal CIS near 26° as well as a shoulder associated with triclinic Cu_2Se at 25.3°. The presence of Cu_2Se arises from the buffer layer deposited before CIS growth but also could be deposited during growth [15]. A progressive increase of the relative intensity of the main CIS peak is observed from the undoped <Li<Na<Cs, suggesting an increase of the film thickness. The peak intensity in CIS:K shows a decrease with respect to CIS:Na, which could be attributed to the reported influence of K on elemental interdiffusion when added during growth [6]. On the other hand, the XRDs presented in Figure 2B display peaks corresponding to Cu_2O at 29.5°, 36.4° and 42.3°, respectively, in all the patterns, but particularly evident in the Cs-doped sample; elementary In is particularly strong in the K-doped sample and a small peak corresponding to CuIn at 34.5° is also evident in the K sample, and both could be attributed to a less complete reaction because the above-mentioned K-dependent hindering of elementary diffusion [9,10]. The presence of Cu_2O would arise from the early oxide formed before deposition, but in the case of the Cs-doped film it is evident that it is mostly formed during growth. In a previous report [11], alkaline-doped Cu_2O films were prepared by anodization. In that report the Cu substrate was first cathodized in order to "load" it with the alkaline ions, before proceeding to anodization. It was observed that film growth was hindered upon strong Cs absorption onto the substrate. In the present report, in contrast, film cathodic deposition seems to be enhanced when Cs is added during growth. According to the early work of R. Notoya [17], the effect could be attributed to Cs^+ adsorption which would lead to a local increase in pH, thus increasing the H_2 evolution overpotential, making more efficient the deposition current and therefore the film thickness. The increase in Cu_2O formation could also be explained by this increase in local pH, where the source of oxygen would be the decomposed water on the adsorbed Cs^+ [17]. Additionally, it is known that alkali metals have a catalytic effect on

semiconductor oxidation as they induce polarization in the O_2 molecule, leading to easily dissociable O_2^- [5]; the effect in the electrolyte solution is the above-described increase in pH upon alkali-catalyzed water dissociation.
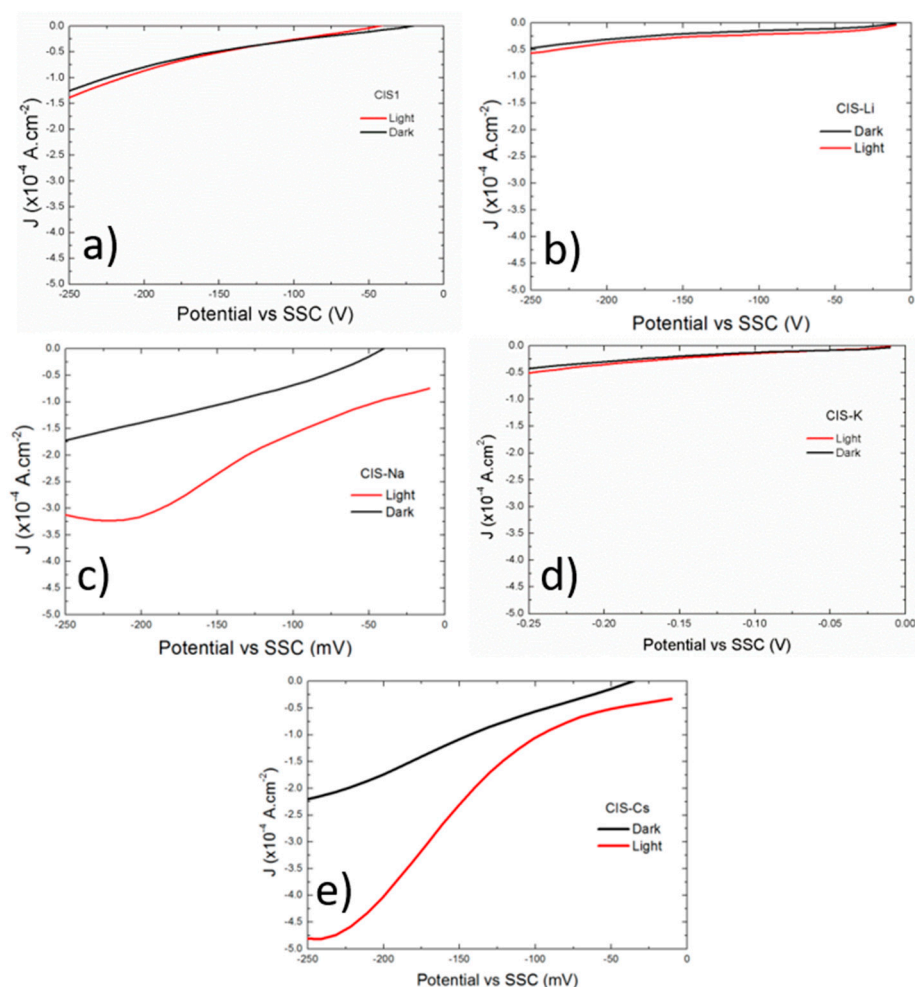
3.2. Photocurrent Response

Figure 3. Photocurrent response of the alkaline-doped CIS films: (**a**) undoped, (**b**) CIS:Li, (**c**) CIS:Na, (**d**) CIS:K, and (**e**) CIS:Cs.

Figure 3 presents the photocurrent response of the films in front of a $NaNO_3$ electrolyte during a continuous potential sweep from OCP to −250 mV vs. the SSC electrode. The films present almost no noticeable photocurrent response (PCR), except for the Na-doped and the Cs-doped films. The lack of PCR can be attributed to the presence of the deleterious Cu_2Se phase within the films [18] as well as metallic phases such as In and CuIn, particularly in the K-doped film. On the other hand, the increase in the photocurrent response in the films doped with Na and Cs could be due to the catalyzed oxidation of the semiconductor surface [5] which leads to Se vacancy neutralization, a well-known recombination center in CI(G)S, and the formation of p-Cu_2O. Therefore, the effect of Na and Cs will overcome the effect of the deleterious Cu_2Se phase through progressive $(Cu_2Se)_{1-x}(Cu_2O)_x$ formation on the Cu_2Se surface, as the relative intensities of the Cu_2O and Cu_2Se/CIS peaks in the Cs- and Na-doped films indicate. In the case of K, the observed formation of metallic phases within the film as well as the proposed $KInSe_2$ compound [9] would deteriorate any photocurrent response, and also there are reports that mention that, in contrast to Na-doping, the beneficial effect of which has been related to V_{Cu} capture and thus Cu mass transport [19], K creates electron traps, particularly on Cu-poor CIS films [20], which would also deteriorate the photocurrent response, as actually observed.

3.3. Electrical Characterization by CAFM

Figure 4 presents the CAFM images of the films, acquired at +100 mV. The figure shows the over-imposed topography and electrical signals. The scheme on the top-left section indicates the expected current flux at the employed bias applying the potential to the sample: holes from the film will flow to the tip. The image corresponding to the undoped film displays the current flowing uniformly mostly through the grain boundaries (GBs). Conversely, the CIS:Li, CIS:Na and CIS:K films display current patches accumulated in some grain junctions, without a uniform distribution, although some conduction through the GBs can be observed. Finally, the image of the CIS:Cs film displays accumulated charges on the grain surfaces, rather than at grain boundaries. The observations indicate that the doping addition during film growth leads to a non-uniform dopant distribution, although the effect of doping on the conductance upon voltage biasing will be discussed below. In the case of Cs-doped CIS, the observations are consistent with the above-discussed Cs^+ adsorption and further formation of Cu_2O on the top of the grains.
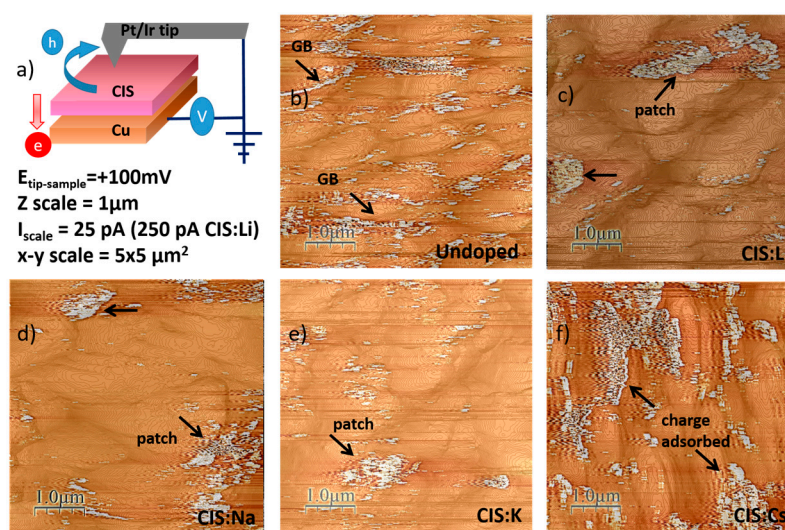

Figure 4. a) Scheme of the setup of the CAFM measurement and summary of experimental conditions and image characteristics. Over-imposed topography and current images of the films. Arrows indicate current flow paths, b) CIS, c) CIS:Li, d) CIS:Na, e) CIS:K, f) CIS:Cs.

Figure 5 presents the averaged and corrected IV curves, where the displayed curves arise from at least 50 curves acquired in three different locations for each sample. The x-y displacements were corrected for the sake of curve fitting from (0,0). The non-corrected curves are presented in the Supplementary Information (Figures S1–S5). In Figure 5, the curve of the undoped film displays a rectifying behavior in a bias range of 0–750 mV, indicating a short space charge layer, compared with the doped films, possibly due to charged defects and foreign phases. The curve corresponding to the Li-doped film presents a rectifying section up to 1700 mV. Another noticeable feature is the large tip-sample current range (up to 12.5 nA) with respect to the undoped film (ca. 100 pA). The higher conductance of the CIS:Li film is possible due to the substitutional incorporation of the Li CIS lattice, leading to an increase in the carrier concentration [18]. The *I–V* curve of the Na-doped film shows an extended, well-defined rectifying behavior up to 3000 mV and a current injection from the contacts above 3000 mV. The current level (12.5 nA) is similar to that of CIS:Li. The literature reports that Na-doping is beneficial for $CuInSe_2$ by creating electrically benign defects that are not electron traps [5,6]. The *I–V* curve of the K-doped CIS film presents very similar characteristics to that of undoped CIS, i.e., rectifying behavior up to 750 mV but a smaller current response, ca. 10 pA vs. 100 pA in the CIS sample, confirming the deleterious effect of K in the electrical behavior, also reflected in the photocurrent response. Finally, the *I–V* curve of the Cs-doped CIS film shows a rectifying behavior up to 1500 mV. Figures S4 and S5 show that both IV curves from CIS:K and CIS:Cs display large

hysteresis as well as *x-y* displacement. The behavior confirms the charge accumulation observed in the CAFM images leading to the formation of surface capacitors. However, as discussed before, only Cs-doping seems to be beneficial for the photocurrent response, although a deeper investigation of Cs incorporation on the electronic properties is needed.
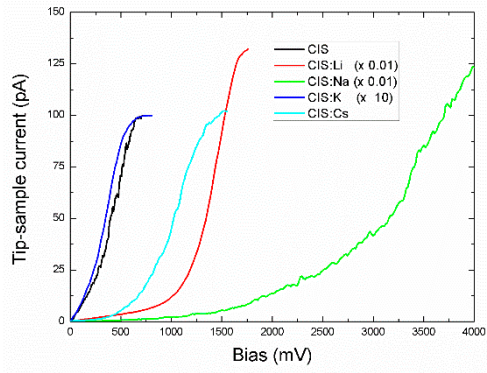

Figure 5. Averaged and corrected CAFM IV curves in the forward sweep and first quadrant of the undoped CIS and alkaline-doped CIS films.

The IV curves were fitted with the Shockley equation.

$$I_D = I_S \left(e^{\frac{V_D}{nV_T}} - 1 \right) \tag{1}$$

where I_s is the inverse saturation current, V_D is the forward bias applied through the diode, n is the ideality factor and V_T is the thermal-dependent voltage determined by kT/q where k is the Boltzmann constant, T is the room temperature and q is the elementary electron charge. The fitting parameters are presented in Table 1. No particular tendency related to ion sizes is observed because of the large dispersion in the *I–V* curves (see Figures S1–S5 in Supplementary information); however, the large values of n indicate the prevalence of tunneling conduction mechanisms rather than thermoionic emission caused by the uneven distribution of dopants incorporated during film growth, as well as by the local variations of surface-accumulated charges observed in the electrical images. Future work is intended to "load" the dopants on the Cu substrate before film growth as reported in [9], although the effect of Cu_2O formation must be assessed as well, as it has been suggested that it could have a beneficial effect in back contacts in CdTe solar cells.

Table 1. Fitting parameters.

Sample	*A* (mV)	I_s (pA)	*n*
CIS	204	21.7 ± 0.7	11.40
CIS:Li	708	490 ± 30	9.78
CIS:Na	60	1079 ± 60	16.24
CIS:K	1022	2.41 ± 0.09	22.5
CIS:Cs	1085	5.4 ± 0.2	10.45

4. Conclusions

Alkaline (Li, Na, K and Cs) doped $CuInSe_2$ films were grown by electrodeposition in a single bath. The ion size influences the photocurrent as well as the dark local current by substitutional incorporation such as with Li or by surface accumulation as in the case of Cs. The reported beneficial effect of sodium upon the photocurrent response was not observed because ion doping was done during the film growth, as the dopant distribution is uneven within the film thickness. From CAFM measurements the local charge segregation was observed, as well as the rectifying behavior. Cesium-doping appears to be very attractive for future applications such as in photocatalytics or

photovoltaics because of the enlargement of the space charge layer by the creation of a capacitive interface.

Author Contributions: L.A.-R. performed the film growth; J.A.B.-M. ran the CAFM and SEM measurements; O.C. simulated and fitted the I-V curves; J.L.F.-M. measured the photocurrent response; C.G.-A. ran the XRD measurements; F.F.C-L. did the data analysis. U.P.-G. and F.C.-B. conceived the experiments and wrote the paper.

Conflicts of Interest: The authors declare no conflict of interest.

References

1.   Shrestha, S. Photovoltaics literature survey. *Prog. Photov Res. Appl*. **2014**, *22*, 502–504.

2.   Wu, Z.M.; Tong, X.; Sheng, P.T.; Li, W.L.; Yin, X.H.; Zou, J.M.; Cai, Q.Y. Fabrication of high-performance $CuInSe_2$ nanocrystals-modified TiO_2 NTs for photocatalytic degradation applications. *Appl. Surf. Sci.* **2015**, *351*, 309–315.

3.   Wilman, S.; Shigeru, I.; Takashi, H.; Masanobu, H.; Ryu, A.; Michio, M. Photosplitting of Water from Wide-Gap Cu(In, Ga)S$_2$ Thin Films Modified with a CdS Layer and Pt Nanoparticles for a High-Onset-Potential Photocathode. *J. Phys. Chem. C* **2015**, *119*, 8576–8583.

4.   Guillemoles, J.F. The puzzle of Cu(In,Ga)Se$_2$ (CIGS) solar cells stability. *Thin Solid Films* **2002**, *403*, 405–409.

5.   Kronik, L.; Cahen, D.; and Werner, S.H. Effects of Sodium on Polycrystalline Cu(In,Ga)Se$_2$ and Its Solar Cell Performance. *ACS Adv. Mater.* **1998**, *10*, 31–36.

6.   Pianezzi, F.; Reinhard, P.; Chirila, A.; Nishiwaki, S.; Bissig, B.; Buecheler, S.; Tiwari, A.N. Defect formation in Cu(In,Ga)Se$_2$ thin films due to the presence of potassium during growth by low temperature co-evaporation process. *J. Appl. Phys.* **2013**, *114*, 194508.

7.   Stange, H.; Brunken, S.; Hempel, H.; Rodriguez-Alvarez, H.; Schafer, N.; Greiner, D.; Scheu, A.; Lauche, J.; Kaufmann, C.A.; Unold, T.; Abou-Ras, D.; Mainz, R. Effect of Na presence during CuInSe$_2$ growth on stacking fault annihilation and electronic properties. *Appl. Phys. Lett.* **2015**, *107*, 152103.

8.   Mishra, S.; Ganguli, B. Effect of structural distortion and nature of bonding on the electronic properties of defect and Li-doped CuInSe$_2$ Chalcopyrite Semiconductors. *J. Alloys Comp.* **2012**, *512*, 17–22.

9.   Laemmle, A.; Wuerz, R.; Powalla, M. Investigation of the effect of potassium on Cu(In,Ga)Se$_2$ layers and solar cells. *Thin Solid Films* **2015**, *582*, 27–30.

10.   Shin, D.; Kim, J.; Gershon, T.; Mankad, R.; Hopstaken, M.; Guha, S.; Tae, A.B.; Shin, B. Effects of the incorporation of alkali elements on Cu(In,Ga)Se$_2$ thin film solar cells. *Sol. Energy Mat. Sol. Cells* **2016**, *157*, 695–702.

11.   Caballero, B.F.; Palacios, P.A.; Calzadilla, O.; Moreira, I. de P.R.; Sanz, F. Disruption of the Chemical Environment and Electronic Structure in p-Type Cu$_2$O Films by Alkaline Doping. *J. Phys. Chem. C* **2012**, *116*, 13524–13535.

12.   Economou, N.J.; Mubeen, S.; Buratto S.K.; McFarland, E.W. Investigation of Arrays of Photosynthetically Active Heterostructures Using Conductive Probe Atomic Force Microscopy. *Nano Lett.* **2014**, *14*, 3328−3334.

13.   Doron, A.; Oded, M.; Isaac, B.; Hans, W.S.; Iris, V.-F.; David, C. Current routes in polycrystalline CuInSe$_2$ and Cu(In,Ga)Se$_2$ films. *Sol. Energy. Mat. Sol. Cells* **2007**, *91*, 85–90.

14.   Tombak, A.; Benhaliliba, M.; Ocak, Y.S.; Kiliçoglu, T. The novel transparent sputtered p-type CuO thin films and Ag/p-CuO/n-Si Schottky diode applications. *Results Phys.* **2015**, *5*, 314–321.

15.   Arvizu-Rodríguez, L.E.; Palacios-Padrós, A.; Chalé-Lara, F.; Fernández-Muñoz, J.L.; Díez-Pérez, I.; Sanz, F.; Espinosa-Faller, F.J.; Sandoval, J.; Caballero-Briones, F. Phase and surface modification by electrochemical post deposition treatments in ultrasonic-assisted CuInSe$_2$/Cu electrodeposited films. *Chalc. Lett.* **2015**, *12*, 537–545.

16.   Caballero, B.F.; Palacios, P.A.; Sanz, F. CuInSe$_2$ films prepared by three step pulsed electrodeposition. Deposition mechanisms, optical and photoelectrochemical studies. *Electrochimica Acta* **2011**, *56*, 9556–9567.

17. Notoya, R. Kinetic studies of electron transfer step of hydrogen evolution reaction on platinum in aqueous cesium hydroxide. *J. Res. Inst. Catal.* **1970**, *9*, 17–28.

18. Hsieh, T.P.; Chuang, C.C.; Wu, C.-S.; Chang, J.C.; Guo, J.-W.; Chen, W.-C. Effects of residual copper selenide on $CuInGaSe_2$ solar cells. *Solid State Electron.* **2011**, *56*, 175–178.

19. Oikkonen, L.E.; Ganchenkova, M.G.; Seitsonen, A.P.; Nieminen, R.M. Effect of sodium incorporation into $CuInSe_2$ from first principles. *J. Appl. Phys.* **2013**, *114*, 083503.

20. Elaheh, G.; Janos, K.; Hossein, M.; Guido, R.; Markus, S.; Johannes, W.; Thomas, D.K.; Claudia, F. Hybrid-Functional Calculations on the Incorporation of Na and K Impurities into the $CuInSe_2$ and $CuIn_5Se_8$ Solar-Cell Materials. *Phys. Chem. C* **2015**, *119*, 25197–25203.